Chemical Science

ROYAL SOCIETY OF CHEMISTRY

EDGE ARTICLE

View Article Online
View Journal | View Issue

Cite this: *Chem. Sci.*, 2024, **15**, 9814

All publication charges for this article have been paid for by the Royal Society of Chemistry

Efficient and stabilized molecular doping of hole-transporting materials driven by a cyclic-anion strategy for perovskite solar cells†

Huaibiao Zeng,[ab] Fangyan Lin,[a] Zhongquan Wan, *[ab] Hua Yang,[c] Hui Lu,[b] Shaoliang Jiang,[a] Jinqing Zhu,[a] Haomiao Yin,[a] Runmin Wei,[b] Yuanxi Wang,[a] Junsheng Luo *[ab] and Chunyang Jia *[ab]

Received 26th March 2024
Accepted 13th May 2024

DOI: 10.1039/d4sc02020k

rsc.li/chemical-science

Bis(trifluoromethane)sulfonimide lithium salt (Li-TFSI) is commonly used as an effective dopant to improve the performance of the hole-transporting material (HTM) in n–i–p perovskite solar cells (PSCs). However, the ultra-hygroscopic and migratory nature of Li-TFSI leads to inferior stability of PSCs. Here, we report on a strategy to regulate the anion unit in Li-TFSI from linear to cyclic, constructing a new dopant, lithium 1,1,2,2,3,3-hexafluoropropane-1,3-disulfonimide (Li-CYCLIC), for the state-of-the-art poly[bis(4-phenyl)(2,4,6-trimethylphenyl)amine] (PTAA). Mechanistic and experimental results reveal that the cyclic anion $CYCLIC^-$ exhibits stronger interaction with Li^+ and $PTAA^{\bullet+}$ compared with the linear anion $TFSI^-$, thus significantly restraining the moisture absorption and migration of Li^+ and improving the thermodynamic stability of $PTAA^{\bullet+}CYCLIC^-$. With this molecular engineering, the resulting PSCs based on Li-CYCLIC obtained an improved efficiency, along with remarkably enhanced stability, retaining 96% of the initial efficiency after over 1150 hours under continuous 1 sun illumination in an N_2 atmosphere, yielding an extrapolated T_{80} of over 12 000 hours. In a broader context, the proposed strategy of linear-to-cyclic doping provides substantial guidance for the subsequent advancement in the development of effective dopants for photoelectric devices.

1. Introduction

Since 2009, the rapid enhancement of power conversion efficiency (PCE) has drawn significant attention to organic–inorganic hybrid perovskite solar cells (PSCs), and their highest efficiency has currently exceeded 26%.[1–7] In regular n–i–p structured PSCs, the polymer poly[bis(4-phenyl)(2,4,6-trimethylphenyl)amine] (PTAA) is widely used as a hole-transporting material (HTM), which facilitates the extraction and transport of holes from the perovskite layer.[8,9] Currently, PTAA adopts a co-doping strategy, usually doping bis(trifluoromethane)sulfonamide lithium salt (Li-TFSI) and 4-*tert*-butylpyridine (*t*-BP) to improve the conductivity, which also brings about significant PCE improvement in PSCs.[10,11] However, the introduction of Li-TFSI affects the long-term stability of PSCs, which is the most challenging issue limiting their commercialization. Ultra-hygroscopic Li-TFSI tends to absorb moisture when devices are exposed to the atmosphere, thus initiating moisture-induced degradation of the hole-transporting layer (HTL) and underlying perovskite layer. In addition, lithium ions with a small van der Waals radius easily migrate from the HTL to the perovskite layer and even the electron-transporting layer (ETL) during the photo-thermal aging process, leading to decreased conductivity of the HTM and thereby accelerating the degradation of PSCs.[12–14] We argue that enhancing the interaction between lithium ions and the anion unit of the dopant is an effective strategy to suppress the moisture absorption and migration of lithium ions, thus enhancing the long-term stability of PSCs.

Herein, a cyclic anion strategy was adopted to tailor the molecular structure of traditional Li-TFSI (Fig. 1a), and a lithium 1,1,2,2,3,3-hexafluoropropane-1,3-disulfonimide dopant (Li-CYCLIC, Fig. 1b) was developed as an alternative to Li-TFSI for PTAA in PSCs. Our design enables the Li-CYCLIC molecule to tackle the challenges of Li^+ hygroscopicity and migration and improve the thermodynamic stability of the $PTAA^{\bullet+}CYCLIC^-$ system that contributes to enhancing the efficiency (22.23%) as well as improving the extrinsic (environmental) and intrinsic (operational) stability of PSCs. The unencapsulated PSCs retain 96% of the original efficiency after aging under 1 sun illumination for 1150 hours in an N_2

[a]National Key Laboratory of Electronic Films and Integrated Devices, School of Integrated Circuit Science and Engineering, University of Electronic Science and Technology of China, 611731 Chengdu, P. R. China. E-mail: zqwan@uestc.edu.cn; luojs@uestc.edu.cn; cyjia@uestc.edu.cn

[b]Shenzhen Institute for Advanced Study, University of Electronic Science and Technology of China, 518110 Shenzhen, P. R. China

[c]Dongguan Neutron Science Center, Dongguan 523803, P. R. China

† Electronic supplementary information (ESI) available. See DOI: https://doi.org/10.1039/d4sc02020k

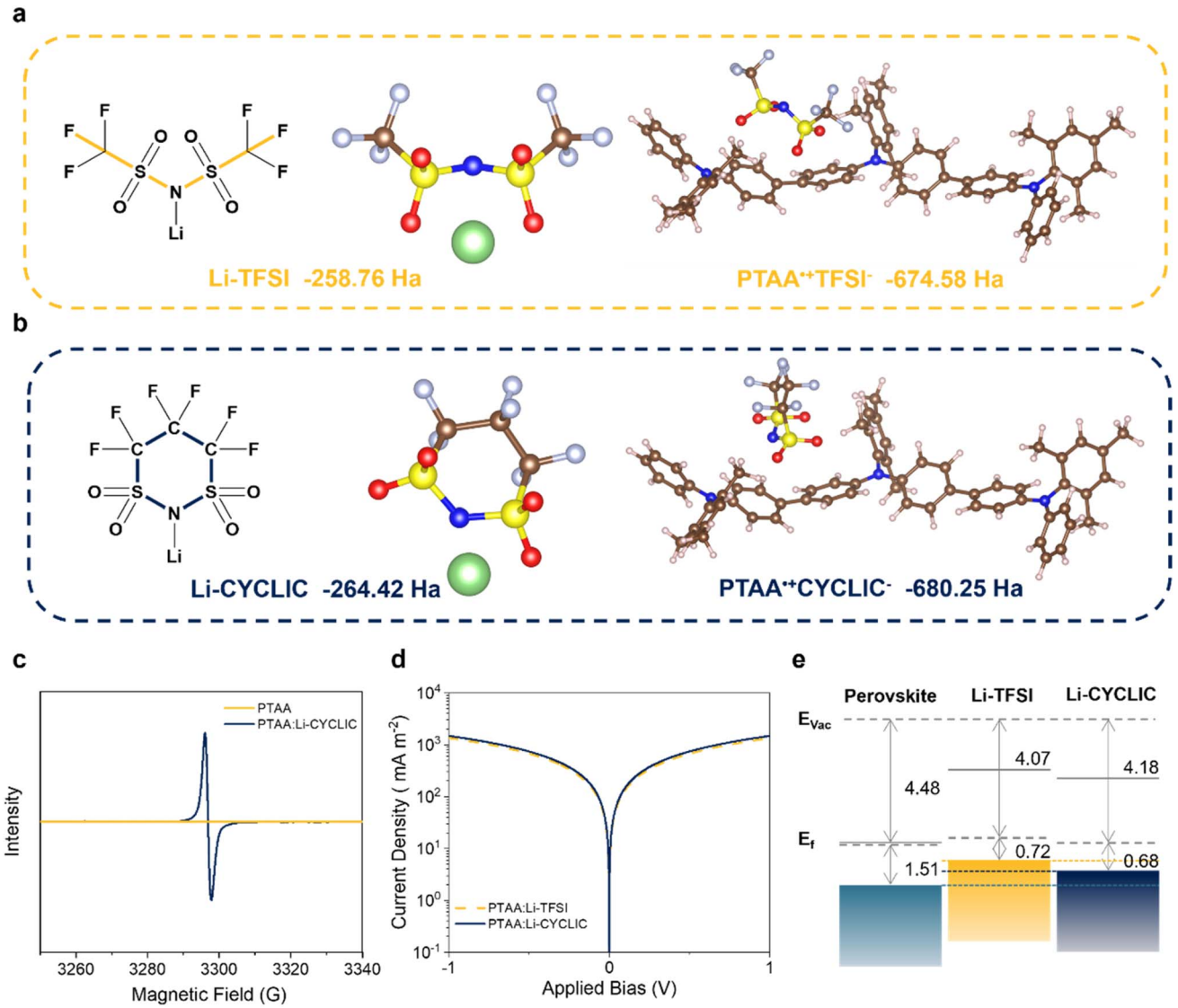

Fig. 1 Molecular formulas and optimized structures with PTAA$^{\bullet+}$ of (a) Li-TFSI and (b) Li-CYCLIC. (c) ESR spectra based on PTAA without or with Li-CYCLIC. (d) Conductivity of PTAA films doped by Li-TFSI and Li-CYCLIC. (e) Energy level alignments of the perovskite and PTAA with Li-TFSI or Li-CYCLIC.

atmosphere and 70% of the initial efficiency after aging for 40 days in the air with relative humidity (RH) of 50–85%.

2. Results and discussion

2.1 Molecular design

To target a desired dopant for PTAA in PSCs, the Li-TFSI backbone is chosen here due to its superior doping performances. However, Li-TFSI usually shows a hygroscopic and migratory nature, which seriously affects the PSC performances when severe operational conditions are applied, such as light, heat and humidity. Therefore, we propose a critical design concept to strengthen the interaction of the anion of the dopant with an Li^+ ion and PTAA radical cation by a linear-to-cyclic anion strategy.

The density functional theory (DFT) calculation results based on the energetic gain show that the total energy of the anion decreases upon regulating the chemical structure from linear ($TFSI^-$, −251.36 Ha) to cyclic ($CYCLIC^-$, −257.03 Ha), correspondingly enhancing the interaction between lithium ions and the cyclic anion (Li-CYCLIC *vs.* Li-TFSI, −264.42 Ha *vs.* −258.76 Ha), as shown in Fig. 1a and b and Table S1.† Fig. S1† shows that the distance of 1.963 Å between Li and N atoms in Li-CYCLIC is shorter than the distance of 1.980 Å in Li-TFSI, which further gives support for the lower total energy of Li-CYCLIC from the perspective of a more stable geometrical structure. This transformation provides effective support for the better hydrophobicity and ion migration limitation ability of Li-CYCLIC in PSCs. In the doping process, the PTAA$^{\bullet+}$ needs to be stabilized by interacting with anions to facilitate the doping reaction; therefore, the different anion structures of Li-TFSI and

Li-CYCLIC will lead to different doping properties and stability. We calculated the total energy values of different forms of dopants during the action process, to evaluate their impact on the stability of the host : dopant system. The total energy of $PTAA^{\bullet+}CYCLIC^{-}$ (−680.25 Ha) is lower than that of $PTAA^{\bullet+}TFSI^{-}$ (−674.58 Ha), which means the cyclic $CYCLIC^{-}$ anion more easily couples with $PTAA^{\bullet+}$ radicals, thus having higher ion-exchange efficiency and $PTAA^{\bullet+}$ radical concentration. As a result, the obtained cyclic anion is expected to be stable to both Li^{+} and $PTAA^{\bullet+}$, which will contribute to doping the HTM and improving the stability of the corresponding devices.

2.2 Doping mechanism analysis

Lewis acids can form complexes with Lewis base polymers through p-type doping. Studies have shown that Li-TFSI can form a charge-transfer complex with the lone electron pair of nitrogen in PTAA, eventually producing $PTAA^{\bullet+}$.[15] The calculations were performed to gain insight into the doping mechanism and electron transfer between PTAA and Li-CYCLIC. Fig. S2a† depicts the surface electrostatic potential (ESP) of Li-CYCLIC; the positive charge is relatively concentrated on Li^{+}. Meanwhile, PTAA is a π–π conjugated polymer, which is an electron-rich system and can be used as a Lewis base.[16] PTAA is easily polarized under ion electrostatics, thus affecting its local charge distribution. Fig. S2b† displays the differential charge diagram, we used the PTAA trimer structure, and electron depletion and accumulation are shown in yellow and blue, respectively. When Li-CYCLIC interacts with PTAA, the holes are mainly localized on the PTAA skeleton, while the electrons are localized on the Li-CYCLIC. This demonstrates that there is a charge transfer between Li-CYCLIC and PTAA, which increases the hole concentration of PTAA molecules, and also represents the generation of $PTAA^{\bullet+}$, thereby achieving effective doping of PTAA.

According to the result of ultraviolet-visible (UV-vis) spectroscopy (Fig. S3†), compared with the dopant-free PTAA solution, the PTAA:Li-CYCLIC solution showed a color shift after illumination, and there was a significant change in the absorption peak at 450 nm in the UV-vis spectrum, which is attributable to the formation of $PTAA^{\bullet+}$. In order to confirm the existence of the doping reaction, electron spin resonance (ESR) can be used to identify the presence of $PTAA^{\bullet+}$ in solution.[17] It can be seen from Fig. 1c that the ESR spectrum of the PTAA solution doped with Li-CYCLIC presents an obvious paramagnetic resonance peak in the range of 3290–3300 G, which indicates the formation of $PTAA^{\bullet+}$ radicals, while the undoped PTAA showed no signal peaks.

As shown in Fig. 1d, the Li-CYCLIC-doped PTAA film (5.18×10^{-3} S m^{-1}) has higher conductivity than the Li-TFSI-doped PTAA film (4.71×10^{-3} S m^{-1}), which can serve as a support for Li-CYCLIC to act as an effective dopant for PTAA in n–i–p type PSCs. The band alignment of the perovskite with adjacent selective HTLs strongly affects device performance. Using the ultraviolet photoelectron spectroscopy (UPS) data in Fig. S4,† combined with the UV-vis result, we plotted the band energy positions and alignments of the doped PTAA film. The PTAA film doped with Li-CYCLIC has a higher work function (4.18 eV) and a deeper highest occupied molecular orbital (HOMO) energy level, the Fermi level is also closer to the HOMO energy level, and the deeper HOMO energy level is more favorable for improving hole injection efficiency and suppressing voltage losses in PSCs.[18] It is obvious that compared with PTAA:Li-TFSI, the band arrangement of PTAA:Li-CYCLIC is better matched with the perovskite, with a smaller energy offset, which facilitates the extraction of holes from perovskites (Fig. 1e).

2.3 Interface charge-transporting properties and defect passivation

The surface defects present on perovskite crystals significantly contribute to the deterioration of PSC performance by promoting charge accumulation, which leads to recombination losses.[19] Therefore, we set Pb vacancy defects caused by the formation of Pb–Pb dimers on the surface of perovskite crystals (001) to deeply explore the passivation mechanism of Li-CYCLIC on the perovskite surface. From Fig. S5a,† the surface charge of the perovskite is mainly concentrated around the Pb–Pb dimer, which easily becomes a non-radiative recombination center. According to the ESP of Li-CYCLIC in Fig. S2a,† on the cyclic anion, the negative charges in the cyclic anion are mainly concentrated on oxygen, which can realize the passivation of Pb vacancy defects. When Li-CYCLIC interacts with the Pb–Pb dimer defect (Fig. S5b†), there is a significant reduction in charge accumulation on the surface of the perovskite crystal. We hereby speculate that the closed cyclic skeleton of Li-CYCLIC enhances the electron attracting-ability of the cyclic anion region and widens the charge density difference between oxygen atoms which does not occur on the cyclic skeleton with Pb defects, thus strengthening the charge transfer process between oxygen atoms and the perovskite surface. This significantly reduces the charge accumulation on the perovskite surface, thereby inhibiting the recombination phenomenon of surface charge on the perovskite.

Then, steady-state photoluminescence (PL) and time-resolved PL (TRPL) analyses were performed on the glass/perovskite, glass/perovskite/PTAA:Li-TFSI, and glass/perovskite/PTAA:Li-CYCLIC films, to explore the carrier dynamics at the HTL and perovskite layer interface.[20] As shown in Fig. 2a, the characteristic fluorescence peak of the perovskite light-absorbing material is at a wavelength of around 764 nm. After the perovskite layer is spin-coated with the HTM, the fluorescence is considerably quenched, indicating holes can effectively be transported from the perovskite layer to the HTL. The more significant fluorescence quenching indicates the more efficient transport of holes. The comparison shows that the fluorescence quenching of the sample doped with Li-CYCLIC is stronger than that of the Li-TFSI-doped sample, proving that Li-CYCLIC-doped PTAA has a more efficient hole extraction ability. At the same time, after Li-CYCLIC is doped into PTAA, the PL peak blue-shifts from 764 nm to 762 nm, indicating that Li-CYCLIC passivates the surface defects of the perovskite, which is consistent with the DFT calculation results.[21] The TRPL results are fitted using a bi-exponential model, and the fitting

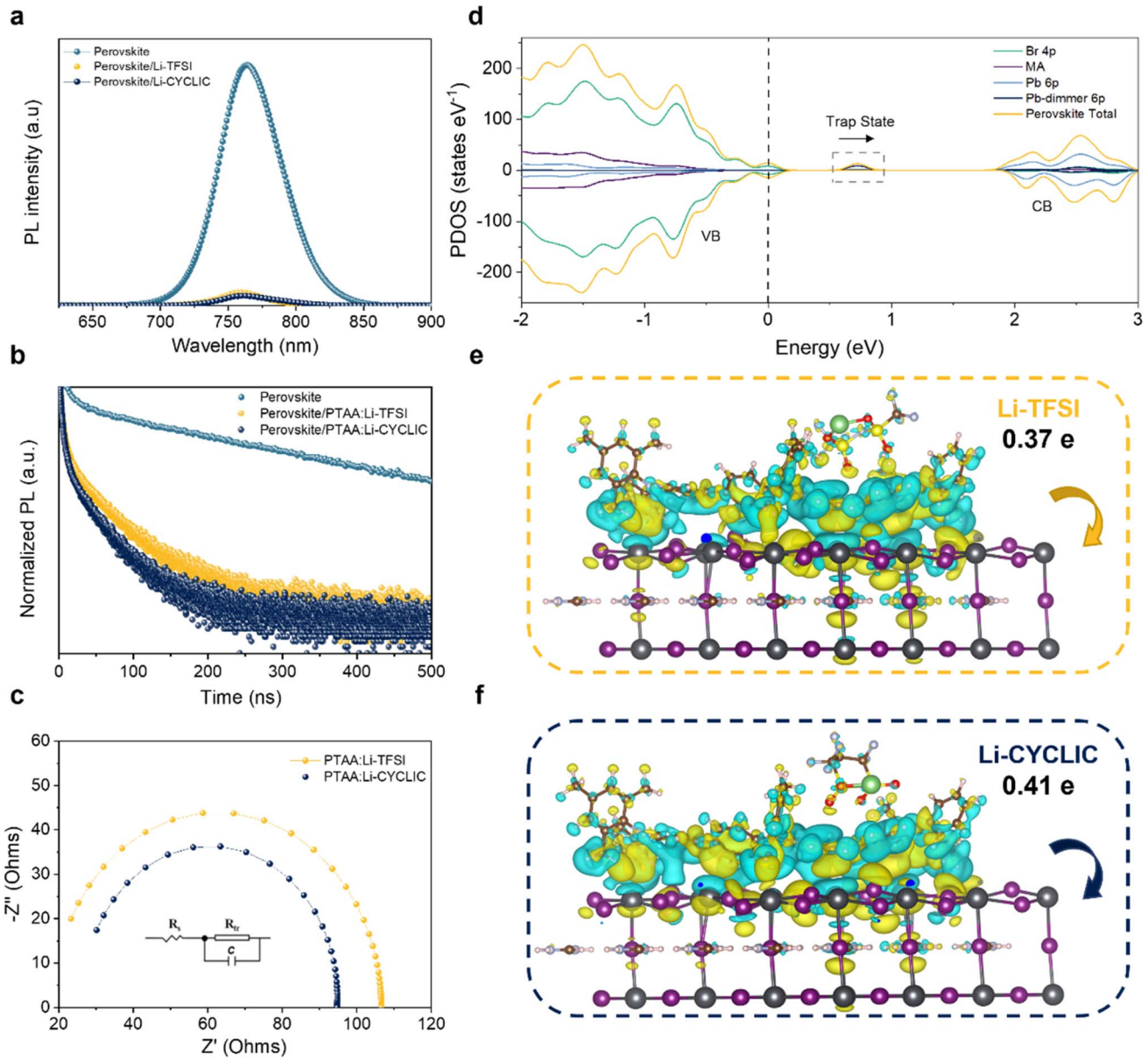

Fig. 2 (a) PL of the perovskite films without or with Li-TFSI and Li-CYCLIC doped PTAA. (b) TRPL decay of the perovskite films without or with Li-TFSI and Li-CYCLIC doped PTAA. (c) Nyquist plots of PSCs based on Li-TFSI and Li-CYCLIC. (d) Perovskite PDOS spectra before and after Li-CYCLIC passivation. Electron transfer between the perovskite and (e) PTAA:Li-TFSI and (f) PTAA:Li-CYCLIC (yellow indicates electron gain and cyan indicates electron loss).

parameters are shown in Table S2.† The TRPL results (Fig. 2b) show that the average decay time (τ_{avg}) of the perovskite film decreases from 210.22 ns to 20.21 ns and 12.31 ns after spin-coating the Li-TFSI doped PTAA and Li-CYCLIC doped PTAA, respectively. The Li-CYCLIC-doped PTAA film has a shorter fluorescence lifetime, indicating that the hole-transporting process is improved. Electrochemical impedance spectroscopy (EIS) was also used to study carrier transport at interfaces. The results of the EIS fitting are shown in Fig. 2c; the inset shows the corresponding fitted circuit diagram. R_{tr} represents the charge transfer resistance at the interface, including the interface between the charge-transporting layer and the perovskite layer, and the interface between the metal electrode and the charge-transport layer. The results indicate that the Li-CYCLIC-based device has a lower R_{tr} value (68.07 Ω) in comparison to the Li-TFSI-based device (88.18 Ω). A lower R_{tr} value signifies a faster charge transfer rate and less charge recombination, which will be reflected in the larger open-circuit voltage (V_{OC}) of the Li-CYCLIC-based device.

We calculated the difference in perovskite density of states pre- and post-passivation to confirm the passivation ability of the dopant. As shown in Fig. 2d, the conduction band mainly consists of Pb 6p orbitals, while Br 4p orbitals dominate the valence band. The existence of Pb vacancy defects introduces

a deep defect state energy level close to the valence band, which consists of the 6p orbital of the Pb–Pb dimer. When Li-CYCLIC interacts with the perovskite, the trap state disappears, and the Pb–Pb dimer peak located at ~0.7 eV disappears. This indicates that there are fewer trap states on the surface of the perovskite films of Li-CYCLIC-doped PTAA. The interaction between Li-CYCLIC and Pb–Pb dimers results in the conversion of deep energy level defects into shallow ones, which highly overlap with the wave function on the perovskite surface to form an impurity energy level. As a result, fewer free charges become trapped, nonradiative recombination weakens, and hole transport improves, leading to an enhancement of the efficiency of PSCs.[22]

To understand the experimental results and the corresponding mechanism of the enhanced passivation by the Li-CYCLIC cyclic structure, we have examined the most stable configurations of Li-TFSI and Li-CYCLIC between the HTL and the perovskite layer and their corresponding total energies (Table S3†) by DFT, respectively. The relaxed models of the perovskite and PTAA with Li-TFSI and Li-CYCLIC are presented in Fig. S6.† Since the configuration with the dopant on top has a lower total energy, we considered this structure to be more stable. Having identified the stable configuration of Li-TFSI and Li-CYCLIC between the HTL and the perovskite layer, Bader charge analysis was performed to study the effects of the two dopants on the interfacial charge transfer process between PTAA and the adjacent perovskite.[23–26] The calculated electron density differences are shown in Fig. 2e and f. PTAA:Li-CYCLIC transfers about 0.41 electrons to the perovskite, while PTAA:Li-TFSI transfers about 0.37 electrons to the perovskite. Combined with the TRPL results, it is shown that the charge transfer process of Li-CYCLIC is significantly enhanced in a shorter time compared to Li-TFSI. Thus, we have shown how Li-CYCLIC affects nonradiative recombination throughout the device and the charge transfer and extraction processes at the interface between the perovskite and the HTL.

2.4 Photovoltaic performances

To study the influence of the linear and cyclic anions of dopants on the device performances, we fabricated and measured PSCs with an n–i–p structure of ITO/SnO_2/perovskite/HTM/Au. The film quality of each layer is intimately related to the performance of PSCs, particularly the perovskite layer where the photoelectric effect occurs. Fig. 3a shows the cross-sectional scanning electron microscope (SEM) image of the complete device architecture. The perovskite layer's good morphology, such as big grains and the intimate contact layers, creates conditions for its excellent photovoltaic performance.

Dopant-free PTAA has a low intrinsic conductivity, and the holes cannot efficiently move through the HTL to the gold electrode in PSCs, causing severe charge recombination, which lowers the short-circuit current density (J_{SC}), V_{OC}, and fill factor (FF).[27] At ambient and 25 °C room temperature without a controlled atmosphere, we measured *J–V* curves. Fig. 3b shows various molarities of Li-CYCLIC (10–20 mol%) that were doped into PTAA solutions to optimize the performance of PSCs. Table S4† gives the corresponding device statistics at each molarity. With the Li-CYCLIC dopant molarity gradually increasing, the efficiency of PSCs improves significantly. As the doping molarity is raised to 20 mol%, the efficiency begins to decline. When 15 mol% was applied, PSCs obtained the maximum efficiency (J_{SC} = 23.96 mA cm^{-2}, V_{OC} = 1.151 V, FF = 80.60%, PCE = 22.23%). The device based on Li-TFSI obtained a lower efficiency (J_{SC} = 23.88 mA cm^{-2}, V_{OC} = 1.133 V, FF = 79.89%, PCE = 21.61%), indicating that Li-CYCLIC exhibits better device performance at the optimized molarity (Fig. 3c). Fig. 3d and S7† compare the photovoltaic parameter distribution of PSCs in the experimental group and the control group, and Table S5† provides the corresponding average values and standard deviation. Devices doped with Li-CYCLIC have better parameter stability and repeatability, J_{SC} = 23.83 ± 0.23 mA cm^{-2}, V_{OC} = 1.140 ± 0.017 V, FF = 80.10 ± 0.83%, PCE = 21.77 ± 0.46%, and all exceed those of the devices based on Li-TFSI.

We examined the incident photon-to-current conversion efficiency (IPCE) spectrum of PSCs to confirm the accuracy of J_{SC} values in *J–V* curves. The calculated integrated J_{SC} value of PSCs with Li-CYCLIC is 23.22 mA cm^{-2} (Fig. 3g), which is close to the J_{SC} measured by the *J–V* curve. The measured steady-state output power of the device at the maximum power point (MPP) (Fig. 3e) can measure the accuracy of the PCE obtained from the *J–V* curve, and the device based on Li-CYCLIC also showed a slower decay with a steady-state PCE of 22.23% after a duration of 300 s, while the device based on Li-TFSI had a lower initial value and a faster output decay with time. Besides, the existence of hysteresis affects the accuracy of device PCE.[28] Under the reverse and forward scanning, the hysteresis of the devices based on both Li-CYCLIC and Li-TFSI is negligible (Fig. 3f and S8, and Table S6†). Therefore, these results demonstrate that Li-CYCLIC has greater potential to improve device performance and process controllability.

2.5 Long-term stability

Long-term stability is crucial for the commercialization of PSCs.[29,30] Most dopants used to enhance the hole-transporting properties of the HTM are hygroscopic, which greatly limits the long-term stable lifetime of the devices. The comparison of the normalized efficiency of Li-TFSI and Li-CYCLIC doped devices is shown in Fig. 4a (unpackaged devices aged for 40 days at RT with RH of 50–85%). The device based on Li-CYCLIC retained about 70% of its initial efficiency, while the efficiency of the device based on Li-TFSI dropped to 49% of its initial value after 40 days of aging. To elucidate the origin of the improved environmental stability of PSCs based on Li-CYCLIC, we first discussed the hygroscopicity of the dopants under ambient air. Fig. S9† shows the perovskite decomposition process of Li-TFSI and Li-CYCLIC in the air by absorbing moisture, indicating that Li-CYCLIC exhibits better hydrophobic properties, which is also conducive to the improvement of the hydrophobicity of the HTL formed by it. Further, we analyzed the HTL and compared PTAA:Li-TFSI and PTAA:Li-CYCLIC films. We compared the water contact angles of the two films (Fig. 4b). The addition of Li-TFSI expands the channels for water and oxygen to penetrate

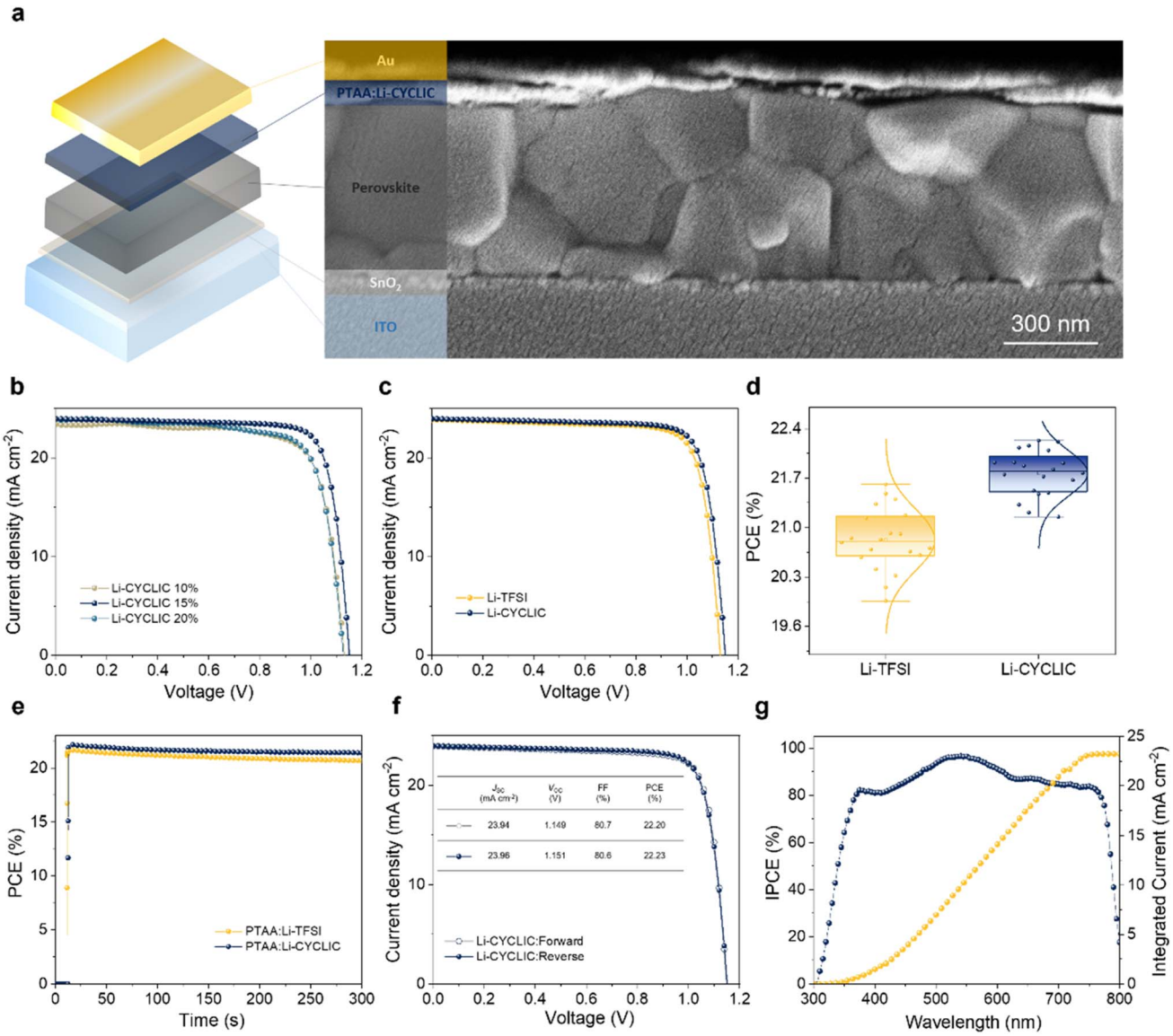

Fig. 3 (a) Structure and cross-sectional SEM image of the PSCs. (b) J–V curves of PSCs based on various molarities of Li-CYCLIC. (c) Best J–V curves of PSCs based on Li-TFSI and Li-CYCLIC. (d) PCE distribution data for PSCs based on Li-TFSI and Li-CYCLIC. (e) Steady-state output of PSCs based on Li-TFSI and Li-CYCLIC. (f) J–V curves of PSCs based on Li-CYCLIC under forward and reverse scans. (g) IPCE spectrum and integrated J_{SC} of PSCs based on Li-CYCLIC.

into PTAA, thus weakening the hydrophobicity of the PTAA film. At the beginning, the PTAA film doped with Li-CYCLIC showed a slight lead in hydrophobicity. As time progressed, the leading trend in hydrophobicity of the PTAA film doped with Li-CYCLIC compared to the PTAA film doped with Li-TFSI expanded, providing support for better environmental stability of the devices based on Li-CYCLIC.

We measure the root mean square roughness (RMS) of the film using an atomic force microscope (AFM) to gauge the quality of the film. The AFM images of the fresh films are shown in Fig. S10.† Compared with the fresh film of PTAA:Li-TFSI (9.4 nm), the fresh film of PTAA:Li-CYCLIC (8.2 nm) has a smaller RMS value and a better surface flatness. Fig. S11† shows the aged SEM morphology of PTAA:Li-TFSI and PTAA:Li-CYCLIC films. The fresh PTAA:Li-CYCLIC film is smooth and flat with no dopant precipitation, which is consistent with the AFM result. After 30 days of aging, the film of PTAA:Li-TFSI showed significant hygroscopic damage on the surface. In comparison, the PTAA:Li-TFSI film showed a slower rate of hygroscopicity and less damage on the surface, indicating that the PTAA:Li-CYCLIC film is more resistant to moisture intrusion. Then, we performed two-dimensional grazing incidence X-ray diffraction (2D-GIXD) on the aged PSCs to present the phase transition of the perovskite crystals during device aging. As shown in Fig. 4d and e, the diffraction peaks at $q \approx 10$, 20, and 22 nm^{-1} correspond to the (110), (220), and (310) crystal planes of perovskite, respectively. The hygroscopicity of Li-TFSI makes the perovskite more susceptible to moisture intrusion, which leads to the

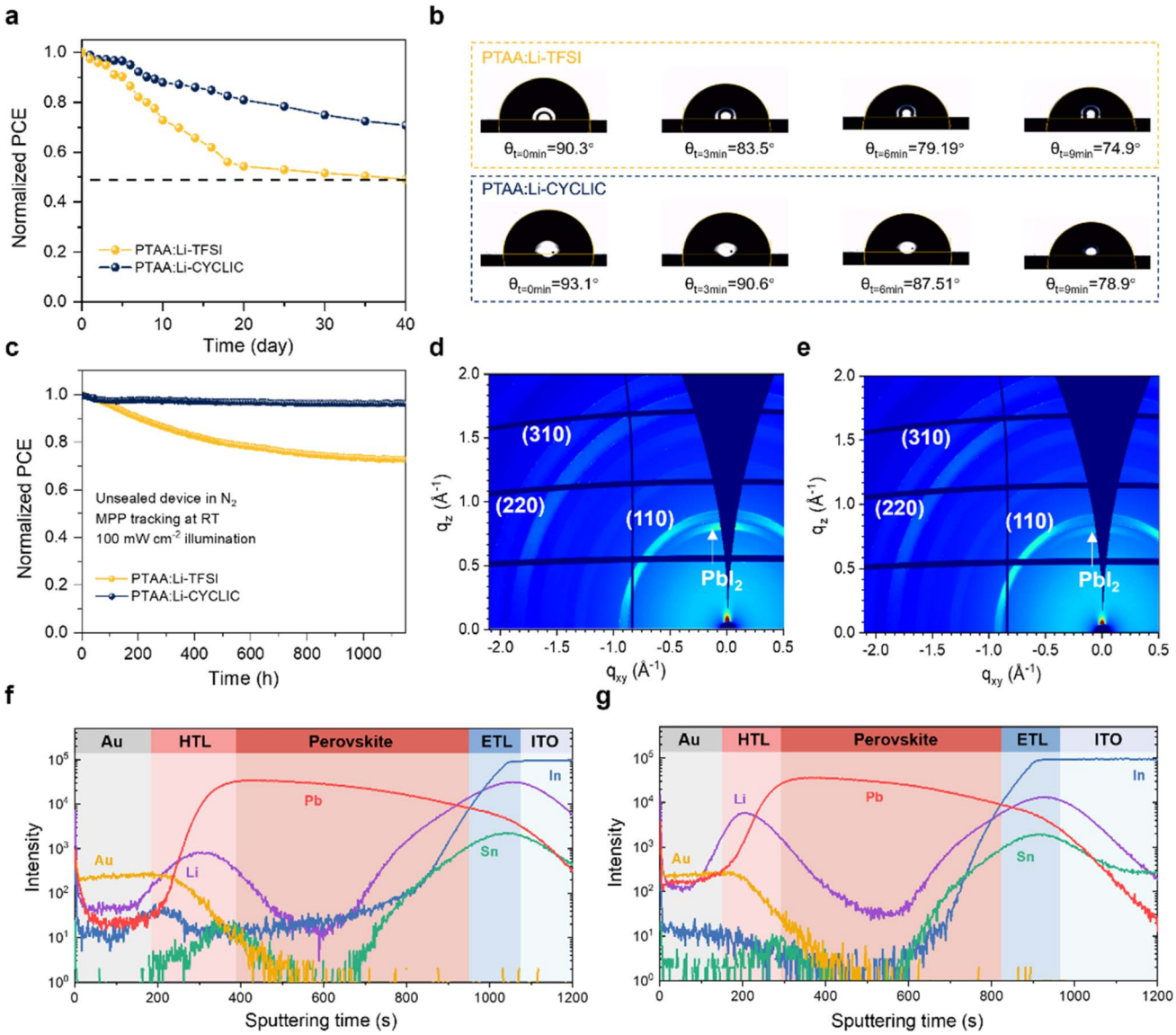

Fig. 4 (a) Normalized efficiency of Li-TFSI and Li-CYCLIC doped devices in ambient air. (b) Water contact angle over time for PTAA:Li-TFSI and PTAA:Li-CYCLIC films. (c) Operational stability of PSCs based on Li-TFSI and Li-CYCLIC under continuous 1 sun illumination in N_2. 2D-GIXD image of the aged device based on (d) Li-TFSI and (e) Li-CYCLIC. TOF-SIMS results of the aged devices based on (f) Li-TFSI and (g) Li-CYCLIC.

decomposition of part of the perovskite to produce PbI_2. PbI_2 is shown as a diffraction peak arising at $q \approx 9$ nm^{-1}, which corresponds to the (001) crystal plane. Thus, the degree of degradation of the perovskite layer can be judged by the intensity of the peak.[31] The PSCs based on Li-CYCLIC exhibit only a weak signal at $q \approx 9$ nm^{-1}, in sharp contrast to the PSCs based on Li-TFSI. This shows that the PSCs based on Li-CYCLIC have better moisture resistance, which reduces the degradation rate of the perovskite. Thus, we have verified the obvious improvement in hydrophobicity of the PSCs based on Li-CYCLIC. We attribute this to the stronger interaction between Li^+ and the cyclic anion (Fig. 1b), which weakens the coordination of Li^+ with H_2O, resulting in better moisture resistance and slower degradation rate of the PSCs based on Li-CYCLIC.[32]

Further, we investigated the operational stability of PSCs under continuous illumination (100 mW cm^{-2}) at room temperature in an N_2 atmosphere according to the International Summit on Organic Photovoltaic Stability protocols (ISOS-L-1). As shown in Fig. 4c, after 1150 hours of continuous testing, the device based on Li-CYCLIC is able to maintain more than 96% of the original PCE, showing good operational stability, while the device based on Li-TFSI shows a severe drop to 72%. We estimate that the time required for the Li-CYCLIC-based devices to drop to eighty percent of its initial performance (T_{80}) is about 12 500 hours (Fig. S12†), demonstrating a 20 times improvement compared with Li-TFSI-based devices ($T_{80} = 500$ hours). We speculate the performance degradation of Li-TFSI-based devices is mainly due to the diffusion of Li^+ in PSCs, which leads to a decrease in the conductivity of the HTL of the corresponding PSCs. Therefore, we examined the migration behavior of ions in the aged device by time-of-flight secondary ion mass spectrometry (TOF-SIMS). In Fig. 4f and g, in the aged

device doped with two dopants, the Li^+ signals are concentrated in the HTL, and then migrate to the perovskite layer across the HTL interface, and finally accumulate in the ETL. It was found that the Li-CYCLIC-based device has a higher concentration of Li^+ in the HTL than the Li-TFSI-based devices, while the Li-TFSI-based device has a higher accumulation concentration of Li^+ in the ETL relative to the Li-CYCLIC-based device (Fig. S13†). Thus, the cyclic anion shows better immobilization ability of Li^+ migration thanks to the stronger interaction in $Li^+CYCLIC^-$ ion pairs, ultimately enhancing the operational stability of PSCs. Meanwhile, lower total energy and more stable $PTAA^{\bullet+}CYCLIC^-$ also contribute to improving the operational stability of devices (Fig. 1b). Thus, our study suggests a unique method to increase the long-term stability of PSCs by increasing the interaction between the dopant and HTM, and alleviating Li^+ ion migration within perovskite devices.

3. Conclusion

In conclusion, we demonstrated a p-type dopant with a cyclic anionic structure, Li-CYCLIC, capable of replacing the classic dopant Li-TFSI in PTAA for PSCs. We have confirmed that the substitution of Li-TFSI with Li-CYCLIC allows a higher conductivity and more favorable band energy alignment of PTAA for efficient extraction of holes from the perovskite layer. Therefore, the corresponding PSCs exhibit lower nonradiative recombination, and stronger interfacial charge transfer capability and subsequently improved photovoltaic performance. Simultaneously, we have found that the cyclic anion has a stronger interaction with lithium ions and the PTAA radical cation, which efficiently suppresses moisture absorption and migration of lithium ions as well as improving the thermodynamic stability of $PTAA^{\bullet+}CYCLIC^-$ compared with the PTAA:Li-TFSI combination, ultimately prolonging the lifetime of the devices. Overall, this work established relationships between the dopant structure and its intrinsic doping and thermodynamic properties, and high-performance PSCs were achieved *via* a cyclic anion strategy, which opens up a unique methodology for discovering new p-type dopants for organic semiconductors and optoelectronic devices.

Data availability

The data that support the findings of this study are available in the ESI.†

Author contributions

J. L. and C. J. conceived the idea for the project. H. Z. and F. L. fabricated and characterized the devices. H. Z., H. L. and F. L. performed and discussed the DFT calculations. F. L. and H. L. helped prepare the 2D-GIXD samples. S. J. and J. Z. performed UPS characterization. R. W., Y. W. and H. Y. participated in the characterization of other properties. H. Y. performed 2D-GIXD. H. Z. and F. L. analyzed all data and wrote the manuscript. J. L. and J. C. conceptualized this work, proposed the logical framework, and revised the manuscript. Z. W. contributed to revising the manuscript. J. C., Z. W. and J. L. directed and supervised the project. All authors discussed the results and commented on the manuscript.

Conflicts of interest

The authors declare no conflict of interest.

Acknowledgements

We are grateful to the National Natural Science Foundation of China (Grant No. 62104031, 22175029 and 62374029), the Technical Field Funds of 173 Project (24JJ210663A), the Sichuan Science and Technology Program (2024NSFSC0250), the Natural Science Foundation of Shenzhen Innovation Committee (No. CYJ20210324135614040), the Foundation of China Petroleum & Chemical Corporation (No. 30000000-23-ZC0607-012736850000-23-ZC0607-0045), the Fundamental Research Funds for the Central Universities of China (No. ZYGX2021J010 and ZYGX2019Z007) and the Open Foundation of State Key Laboratory of Electronic Thin Films and Integrated Devices (KFJJ202109) for financial support.

References

1 A. Kojima, K. Teshima, Y. Shirai and T. Miyasaka, *J. Am. Chem. Soc.*, 2009, **131**, 6050–6051.
2 J. Burschka, N. Pellet, S. J. Moon, R. Humphry-Baker, P. Gao, M. K. Nazeeruddin and M. Grätzel, *Nature*, 2013, **499**, 316–319.
3 Y. Hou, X. Du, S. Scheiner, D. P. McMeekin, Z. Wang, N. Li, M. S. Killian, H. Chen, M. Richter, I. Levchuk, N. Schrenker, E. Spiecker, T. Stubhan, N. A. Luechinger, A. Hirsch, P. Schmuki, H. P. Steinrück, R. H. Fink, M. Halik, H. J. Snaith and C. J. Brabec, *Science*, 2017, **358**, 1192–1197.
4 M. Kim, S. G. Motti, R. Sorrentino and A. Petrozza, *Energy Environ. Sci.*, 2018, **11**, 2609–2619.
5 J. Luo, B. Liu, H. Yin, X. Zhou, M. Wu, H. Shi, J. Zhang, J. Elia, K. Zhang, J. Wu, Z. Xie, C. Liu, J. Yuan, Z. Wan, T. Heumueller, L. Lüer, E. Spiecker, N. Li, C. Jia, C. J. Brabec and Y. Zhao, *Nat. Commun.*, 2024, **15**, 2002.
6 J. Jeong, M. Kim, J. Seo, H. Lu, P. Ahlawat, A. Mishra, Y. Yang, M. A. Hope, F. T. Eickemeyer, M. Kim, Y. J. Yoon, I. W. Choi, B. P. Darwich, S. J. Choi, Y. Jo, J. H. Lee, B. Walker, S. M. Zakeeruddin, L. Emsley, U. Rothlisberger, A. Hagfeldt, D. S. Kim, M. Grätzel and J. Y. Kim, *Nature*, 2021, **592**, 381–385.
7 J. Park, J. Kim, H. S. Yun, M. J. Paik, E. Noh, H. J. Mun, M. G. Kim, T. J. Shin and S. I. Seok, *Nature*, 2023, **616**, 724–730.
8 J. Kong, Y. Shin, J. A. Röhr, H. Wang, J. Meng, Y. Wu, A. Katzenberg, G. Kim, D. Y. Kim, T. D. Li, E. Chau, F. Antonio, T. Siboonruang, S. Kwon, K. Lee, J. R. Kim, M. A. Modestino, H. Wang and A. D. Taylor, *Nature*, 2021, **594**, 51–56.

9 S. Song, E. Y. Park, B. S. Ma, D. J. Kim, H. H. Park, Y. Y. Kim, S. S. Shin, N. J. Jeon, T. S. Kim and J. Seo, *Adv. Energy Mater.*, 2021, **11**, 9.
10 L. Caliò, M. Salado, S. Kazim and S. Ahmad, *Joule*, 2018, **2**, 1800–1815.
11 K. Wang, X. Liu, R. Huang, C. Wu, D. Yang, X. Hu, X. Jiang, J. C. Duchamp, H. Dorn and S. Priya, *ACS Energy Lett.*, 2019, **4**, 1852–1861.
12 F. Lin, J. Luo, Y. Zhang, J. Zhu, H. A. Malik, Z. Wan and C. Jia, *J. Mater. Chem. A*, 2023, **11**, 2544–2567.
13 L. L. Jiang, Z. K. Wang, M. Li, C.-H. Li, P. F. Fang and L. S. Liao, *J. Mater. Chem. A*, 2019, **7**, 3655–3663.
14 C. Ran, J. Xu, W. Gao, C. Huang and S. Dou, *Chem. Soc. Rev.*, 2018, **47**, 4581–4610.
15 Y. Kim, E. H. Jung, G. Kim, D. Kim, B. J. Kim and J. Seo, *Adv. Energy Mater.*, 2018, **8**, 1801668.
16 F. M. Rombach, S. A. Haque and T. J. Macdonald, *Energy Environ. Sci.*, 2021, **14**, 5161–5190.
17 P. Zalar, M. Kuik, Z. B. Henson, C. Woellner, Y. Zhang, A. Sharenko, G. C. Bazan and T. Q. Nguyen, *Adv. Mater.*, 2014, **26**, 724–727.
18 S. M. Park, S. M. Mazza, Z. M. Liang, A. Abtahi, A. M. Boehm, S. R. Parkin, J. E. Anthony and K. R. Graham, *ACS Appl. Mater. Interfaces*, 2018, **10**, 15548–15557.
19 L. K. Ono and Y. Qi, *J. Phys. Chem. Lett.*, 2016, **7**, 4764–4794.
20 Z. L. Zhu, J. A. Ma, Z. L. Wang, C. Mu, Z. T. Fan, L. L. Du, Y. Bai, L. Z. Fan, H. Yan, D. L. Phillips and S. H. Yang, *J. Am. Chem. Soc.*, 2014, **136**, 3760–3763.
21 J. X. Xia, J. S. Luo, H. Yang, F. J. Zhao, Z. Q. Wan, H. A. Malik, Y. Shi, K. L. Han, X. J. Yao and C. Y. Jia, *Adv. Funct. Mater.*, 2020, **30**, 14.
22 S. Mahesh, J. M. Ball, R. D. J. Oliver, D. P. McMeekin, P. K. Nayak, M. B. Johnston and H. J. Snaith, *Energy Environ. Sci.*, 2020, **13**, 258–267.
23 W. Tang, E. Sanville and G. Henkelman, *J. Phys.: Condens. Matter*, 2009, **21**, 7.
24 Y. Wang, T. Gould, J. F. Dobson, H. M. Zhang, H. G. Yang, X. D. Yao and H. J. Zhao, *Phys. Chem. Chem. Phys.*, 2014, **16**, 1424–1429.
25 S. N. Yun, X. Zhou, J. Even and A. Hagfeldt, *Angew. Chem., Int. Ed.*, 2017, **56**, 15806–15817.
26 W. Chen, Y. C. Zhou, L. J. Wang, Y. H. Wu, B. Tu, B. B. Yu, F. Z. Liu, H. W. Tam, G. Wang, A. B. Djurisic, L. Huang and Z. B. He, *Adv. Mater.*, 2018, **30**, 9.
27 L. Calió, S. Kazim, M. Grätzel and S. Ahmad, *Angew. Chem., Int. Ed.*, 2016, **55**, 14522–14545.
28 Y. G. Rong, Y. Hu, S. Ravishankar, H. W. Liu, X. M. Hou, Y. S. Sheng, A. Y. Mei, Q. F. Wang, D. Y. Li, M. Xu, J. Bisquert and H. W. Han, *Energy Environ. Sci.*, 2017, **10**, 2383–2391.
29 I. M. Peters, J. Hauch, C. Brabec and P. Sinha, *Joule*, 2021, **5**, 3137–3153.
30 J. P. Correa-Baena, M. Saliba, T. Buonassisi, M. Grätzel, A. Abate, W. Tress and A. Hagfeldt, *Science*, 2017, **358**, 739–744.
31 J. X. Xia, R. L. Zhang, J. S. Luo, H. Yang, H. Y. Shu, H. A. Malik, Z. Q. Wan, Y. Shi, K. L. Han, R. L. Wang, X. J. Yao and C. Y. Jia, *Nano Energy*, 2021, **85**, 12.
32 T. Wang, Y. Zhang, W. Y. Kong, L. Qiao, B. G. Peng, Z. C. Shen, Q. F. Han, H. Chen, Z. L. Yuan, R. K. Zheng and X. D. Yang, *Science*, 2022, **377**, 1227–1231.